Available online at www.sciencedirect.com

ScienceDirect

MATTER AND RADIATION AT EXTREMES

Matter and Radiation at Extremes 3 (2018) 248–255

www.journals.elsevier.com/matter-and-radiation-at-extremes

Research Article

Numerical studies on the radiation uniformity of Z-pinch dynamic hohlraum

Fuyuan Wu [a,b,c], Yanyun Chu [b], Rafael Ramis [c], Zhenghong Li [b,*], Yanyun Ma [a,d,**], Jianlun Yang [b], Zhen Wang [b], Fan Ye [b], Zhanchang Huang [b], Jianmin Qi [b], Lin Zhou [b], Chuan Liang [b], Shijia Chen [a], Zheyi Ge [a], Xiaohu Yang [a], Shangwu Wang [a]

[a] *College of Liberal Arts and Sciences, National University of Defense Technology, Changsha, 410073, China*
[b] *Institute of Nuclear Physics and Chemistry, China Academy of Engineering Physics, Mianyang, 621900, China*
[c] *E.T.S.I. Aeronáuticos y del Espacio, Universidad Politécnica de Madrid, Madrid, 28040, Spain*
[d] *IFSA Collaborative Innovation Center, Shanghai Jiao Tong Univeristy, Shanghai, 200240, China*

Received 11 October 2017; revised 6 May 2018; accepted 15 June 2018
Available online 19 July 2018

Abstract

Radiation uniformity is important for Z-pinch dynamic hohlraum driven fusion. In order to understand the radiation uniformity of Z-pinch dynamic hohlraum, the code MULTI-2D with a new developed magnetic field package is employed to investigate the related physical processes on Julong-I facility with drive current about 7–8 MA. Numerical simulations suggest that Z-pinch dynamic hohlraum with radiation temperature more than 100 eV can be created on Julong-I facility. Although some X-rays can escape out of the hohlraum from Z-pinch plasma and electrodes, the radiation field near the foam center is quite uniform after a transition time. For the load parameters used in this paper, the transition time for the thermal wave transports from $r = 1$ mm to $r = 0$ mm is about 2.0 ns. Implosion of a testing pellet driven by cylindrical dynamic hohlraum shows that symmetrical implosion is hard to achieve due to the relatively slow propagation speed of thermal wave and the compression of cylindrical shock in the foam. With the help of quasi-spherical implosion, the hohlraum radiation uniformity and corresponding pellet implosion symmetry can be significantly improved thanks to the shape modulation of thermal wave front and shock wave front.

PACS codes: 52.58.Lq; 52.59.Qy; 52.65.Kj

Keywords: Z-pinch; Dynamic hohlraum; Radiation uniformity; Shock wave; Thermal wave

1. Introduction

Typical inertial confinement fusion (ICF) schemes involve symmetrical implosions of a fuel-filled capsule or tube driven by laser beams [1,2], ion beams [3], or Z-pinches [4]. Z-pinches are regarded as promising approaches for ICF because of the capability to convert electrical energy into X-ray radiation energy with high efficiency. In the experiments conducted on Z machine located at Sandia National Laboratories, X-ray output as high as 200 TW and 1.8 MJ was produced, with a conversion efficiency from electrical energy to X-ray energy up to 15% [5]. In the past decades, Z-pinch dynamic hohlraum has been used to drive DD pellets on the 20 MA Z machine [6,7], achieving a thermonuclear neutron yield up to 3.1×10^{11}. In the design of next generation Z-pinch facilities, dynamic hohlraum is considered as one of the two candidate loads [8].

A typical Z-pinch dynamic hohlraum is composed of a tungsten wire array and a low density plastic foam. When the high speed tungsten plasma accelerated by Lorentz force is impacting onto the plastic foam, a radiating shock traveling towards the axis is launched, emitting intense X-rays. The X-

* Corresponding author.
** Corresponding author.
E-mail addresses: lee_march@sina.com (Z. Li), yanyunma@126.com (Y. Ma).

Peer review under responsibility of Science and Technology Information Center, China Academy of Engineering Physics.

https://doi.org/10.1016/j.mre.2018.06.001

rays are trapped by the imploding plasma and electrodes, thus a Z-pinch dynamic hohlraum is created. As in the concept of laser driven hohlraum [1], the X-ray radiation inside the Z-pinch dynamic hohlraum can also be used to implode a pellet to fusion conditions.

However, there are some issues to be considered carefully, apart from the effects of magnetic Rayleigh-Taylor instability. First, the spherical pellet will be compressed by the cylindrical shock launched by the collision of the wire arrays and the plastic foam, unless the pellet can be imploded to fusion conditions before the arrival of the shock. Second, some people worry about the radiation uniformity in the Z-pinch dynamic hohlraum, which is a requirement for the symmetrical pellet implosion. This is because that X-rays are emitted by the cylindrical plasma and can escape from the hohlraum at the relatively cool electrode plates.

For Z machine with peak drive current about 20 MA, there have been some 2D integrated simulations along with experiments. For example, Lemke et al. found that the growth of MRT instability had minor effect on the radiation uniformity [9]. Slutz et al. found that the pellet implosions were asymmetric with a ratio of the equatorial/polar radii about 0.7−0.8 at the time of peak fuel temperature [10]. For Julong-I facility [11] with a drive current of 7−8 MA, several simulations and experiments [12−16] have also been performed. For example, Xiao et al. found that mass ratio and radius ratio of Z-pinch plasma and plastic foam should be carefully selected for the trade-off between peak radiation temperature and radiation pulse duration [12]. However, most of the simulations are one-dimensional and few literatures focus on the hohlraum radiation uniformity in the *R-Z* plane until this moment. To get better understanding of radiation uniformity of the hohlraum with/without a pellet on Julong-I facility, calculations using the code MULTI-2D [17] with a new developed magnetic field package [18] are presented herein.

The traditional cylindrical hohlraum is deformed into quasi-spherical hohlraum to improve the radiation uniformity in this work. In the past decades, quasi-spherical implosions are mainly designed to increase the energy density inside the hohlraum due to its three-dimensional compression [19−22], and attentions are paid to make the Z-pinch plasma implode onto a spherical surface simultaneously [23,24]. We shall show that the radiation uniformity could be improved due to the shape modulation of thermal wave front and shock front.

This paper is organized as follows. Sec. 2 describes the physical model of code MULTI-2D. Subsection 3.1 investigates the radiation field uniformity in cylindrical hohlraum without pellet, subsection 3.2 studies the radiation uniformity with a pellet, and in subsection 3.3, the radiation uniformity near the pellet is improved by a quasi-spherical implosion. Finally, Sec. 4 gives the conclusions.

2. Physical model

We employed the open-source radiation hydrodynamics program MULTI-2D with an additional MHD package to perform the simulations. This paper will give a brief introduction of the physical model. For details, please refer to Ref. [17] for the radiation hydrodynamics model and Ref. [18] for the magneto-hydrodynamics model.

MULTI-2D describes hydrodynamics in two spatial dimensions (cylindrical *ZR* geometry) and radiation transport along rays in three dimensions with the 4π solid angle discretized in several directions. The non-structured grid composed of trilateral and quadrilateral cells allows people simulating spherical pellet implosion inside a cylindrical hohlraum, the typical configuration in laser indirectly driven fusion or Z-pinch dynamic hohlraum driven fusion. The radiation transport algorithm can correctly handle optically thick and optically thin regions at the same time. For optically thick region, the radiation mean free path is much smaller than the characteristic length, the radiation transport treatment is equivalent to the diffusive model. Heat conduction model with a flux limiter is implemented in the code as well. The temperatures of the electrons and the ions are regarded as equal. Tabulated equations of state are generated by the QEOS model or the ideal gas model. Either pure Lagrangian mode or Arbitrary Lagrangian-Eulerian (ALE) mode with first-order remapping scheme is available. Since MRT instability is not considered in this work and it is more convenient to track material interfaces in Lagrangian mode, only Lagrangian mode is selected.

After introducing the azimuthal magnetic field into code MULTI-2D, the equations of momentum, internal energy, magnetic field, current density, and radiation transport in cylindrical coordinates are given by

$$\rho\frac{\mathrm{d}\boldsymbol{u}}{\mathrm{d}t} = -\nabla(p+p_\upsilon) - \nabla p_\mathrm{m} - \frac{\boldsymbol{B}^2}{\mu_0 r}\boldsymbol{e}_r \tag{1}$$

$$\rho\frac{\mathrm{d}e}{\mathrm{d}t} = -(p+p_\upsilon)\nabla\cdot\boldsymbol{u} - \nabla\cdot\boldsymbol{q} + \int_{4\pi}\frac{I-I^\mathrm{P}}{\lambda} + Q + \eta\boldsymbol{J}^2, \tag{2}$$

$$\frac{\partial\boldsymbol{B}}{\partial t} = \nabla\times(\boldsymbol{u}\times\boldsymbol{B} - \eta\boldsymbol{J}), \tag{3}$$

$$\boldsymbol{J} = \frac{1}{\mu_0}\nabla\times\boldsymbol{B}, \tag{4}$$

$$\boldsymbol{n}\cdot\nabla I = \frac{I^\mathrm{P}-I}{\lambda}, \tag{5}$$

where ρ is the density, $\boldsymbol{u}$ is the velocity, p is the thermal pressure, p_υ is the artificial viscosity pressure, $p_\mathrm{m} = B^2/2\mu_0$, is the magnetic pressure, $\boldsymbol{B}$ is the magnetic field, $\boldsymbol{\mu}_0$ is the permeability of vacuum, r is the radius, $\boldsymbol{e}_r$ is the unit vector in radius direction, e is the specific internal energy, $\boldsymbol{q}$ is thermal flux, I ($\boldsymbol{n}$, $\boldsymbol{r}$, t) is the radiation intensity (integrated in frequency), $\boldsymbol{n}$ is a unitary vector in the direction of radiation propagation, I^P is the Planck intensity, λ is the radiation mean free path, Q is the energy deposited by external sources such as laser beams or heavy ion beams, η is Spitzer electrical resistivity, $\boldsymbol{J}$ is the electrical current density.

Based on the above descriptions, one can notice that the code MULTI-2D employs a simpler physical model than that

adopted by the one-dimensional version MULTI-IFE [25]. For example, the ions and electrons are assumed to have the same temperature rather than two temperatures, and X-ray radiation is treated as one-group photons rather than multi-group photons. Besides, analytical expressions, rather than tables generated by code SNOP, are adopted for matter opacities. However, since code MULTI-2D is able to perform calculations in two dimensions, the radiation uniformity in *ZR* plane can be evaluated directly, and complicated configurations composed of spherical capsule and cylindrical hohlraum can be simulated. Our previous study [26] also show that the ion temperature and the electron temperature inside the hohlraum do not differ too much even at the position of shock front for Julong-I facility.

3. Calculation results

3.1. Radiation uniformity of cylindrical hohlraum without a pellet

We first investigate the radiation uniformity of Z-pinch dynamic hohlraum in absence of a pellet, using the typical experimental parameters for Julong-I facility. As shown in Fig. 1, the load is 15 mm long, the tungsten plasma shell has a radius of 10 mm, a thickness of 1 mm, a mass of 1.31 mg/cm, and a temperature of 1 eV. The CH plastic foam has a radius of 3 mm, a density of 10 mg/cm^3, and a temperature of 0.1 eV. The drive current is set as

$$I(t) = 7[\mathrm{MA}]\sin^4(\pi t[\mathrm{ns}]/280) \quad (6)$$

The foam radius and foam density are selected based on the following considerations. First, this radius (3 mm) provides enough time for the observation of shock propagation in the foam while ensures the wire array plasma colliding with the foam with a relatively high imploding velocity (~2.2×10^7 cm/s at 140 ns). Second, for this relative low foam density (10 mg/cm^3), the thermal wave is able to travel much faster than the shock wave so that an obvious separation of thermal wave and shock wave can be expected.

The wire array used on Julong-I (7–8 MA) facility is usually composed of large numbers of wires with wire gap less than 1.4 mm, typically 168 wires for an array with a diameter 20 mm. This kind of wire array with small inter-wire gap tends to merge into an annular plasma shell before significant implosion, as reported by Sanford et al. [27] on the 7 MA Saturn facility. However, recent experiments at 1 MA currents on Magpie, Cobra and Zebra facilities show that the wire array implodes in a snow-plow model [28]. First, the wire array undergoes a long ablation phase, filling the space inside the wire array with the low-density ablated plasma streaming to the axis. Later, the wire core mass implodes through the ablated mass layer. It is found that the wire ablation can delay the array stagnation by 15–25 ns on Cobra [29]. Since the wire initiation process cannot be simulated completely by our 2D hydrodynamics code, we start the calculation with approximations similar to that adopted by Slutz et al. [10], assuming some of the array mass is uniformly distributed inside the shell with zero velocity. Knowing that wire array implosions are more complicated than simple annular plasma implosions, we wish to investigate the effects of wire ablation on dynamic hohlraum performance when a 3D magneto-hydrodynamics code and related matter property tables are available in the future.

X-rays inside the hohlraum are mainly generated during the collision of imploding array plasma and plastic foam. Greatly ionized plasmas of high temperature and high density are firstly created during deceleration of the array plasma, then the intense X-rays are emitted when the ionized dense plasma recombines [30]. The radiation temperature distribution in *ZR* plane at 158 ns is presented in Fig. 2. It is shown that the radiation field near the foam center is almost uniform, although there are sharp temperature gradients in the tungsten plasma due to radiation cooling. The radiation temperature in the foam center is about 100 eV while the radiation temperature in the tungsten plasma is about 50 eV. Because the

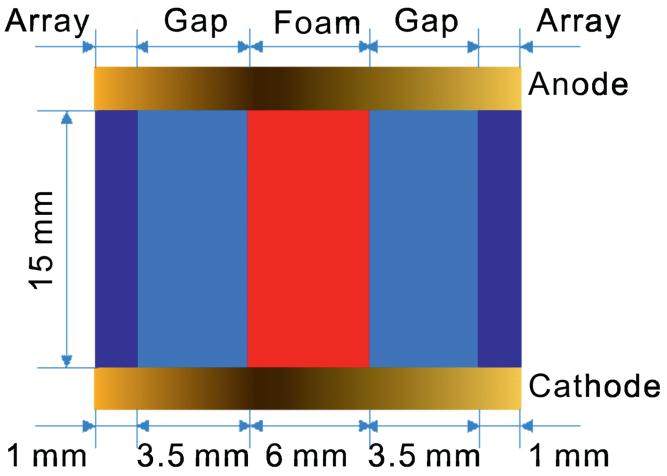

Fig. 1. Schematic diagram of Z-pinch dynamic hohlraum.

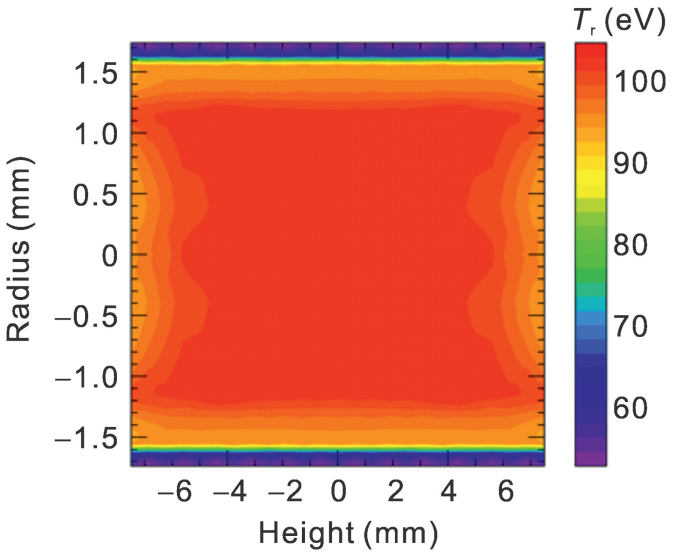

Fig. 2. Radiation temperature distribution in *ZR* plane at 158 ns.

electrode plates are not included in the simulations and X-rays can escape from the hohlraum freely at the two ends in axial direction, the radiation temperature decreases significantly at the two ends. From Fig. 2, one can infer that one-dimensional models used in target design should be valid on the whole, where the pellet is assumed to be ablated by a uniform X-ray radiation field.

Fig. 3 presents the evolutions of radiation temperature on the equator ($r = 1$ mm, $z = 0$ mm) and pole ($r = 0$ mm, $z = 1$ mm) of a virtual pellet (an imaginary region used for radiation uniformity analysis). It is shown that the radiation temperature starts to rise rapidly due to the arrival of thermal wave, on the equator and poles at 154 ns and 156 ns, respectively. After a transition phase lasting 2.0 ns, the radiation temperatures on the equator and pole are almost the same during 157 ns and 159 ns, indicating the radiation field inside the hohlraum is quite uniform during this time. When the shock front passes through the equator at 159 ns, the radiation temperature on the equator is smaller than that on the pole. This is partially because that the X-ray radiation outside the shock front can escape from the hohlraum more easily than that inside the shock front, since the shocked foam is optically thick at this radiation temperature and can provide additional radiation confinement.

3.2. Radiation uniformity of cylindrical hohlraum with a pellet

In subsection 3.1, we demonstrate that a uniform hohlraum radiation field near the foam center can be obtained after a transition time in the absence of pellets. However, in real Z-pinch dynamic hohlraum driven fusion, a fuel-filled pellet presents inside the foam and is supposed to be imploded spherically by the hohlraum radiation field before the arrival of cylindrical shock. It would be interesting to use a pellet implosion to test the radiation uniformity inside the hohlraum.

The initial configuration is illustrated in Fig. 4. The tungsten wire array plasma (in light blue) is 1 eV in temperature,

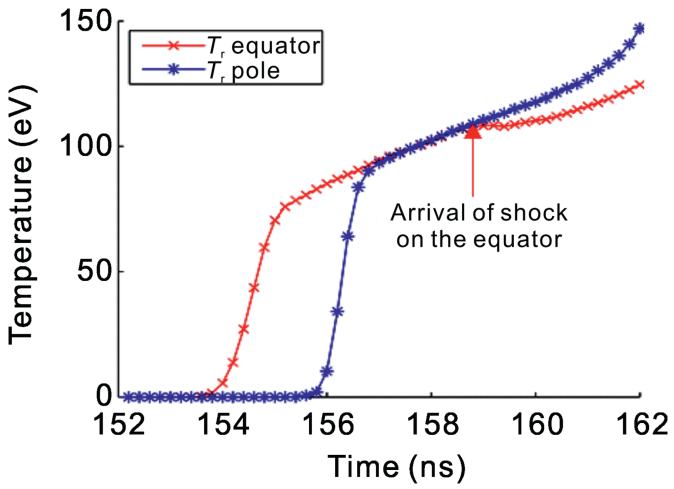

Fig. 3. Evolution of radiation temperature on the equator ($r = 1$ mm, $z = 0$ mm) and pole ($r = 0$ mm, $z = 1$ mm) of a virtual pellet.

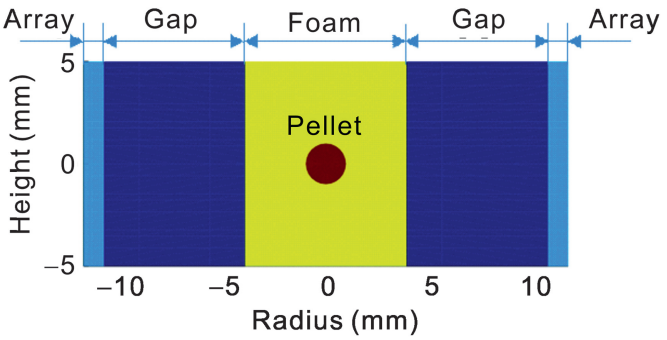

Fig. 4. Schematic of cylindrical hohlraum driven pellet implosion.

1.38 mg/cm in density, 12 mm in radius, 10 mm in height, and 1 mm in thickness. The CH plastic foam (in yellow) is 4 mm in radius, and 5 mg/cm^3 in density. The testing pellet (in red) is made of CH foam, with a radius of 1 mm and a density of 50 mg/cm^3. The drive current is set as $I(t) = 8$ [MA] $\sin^4$ (πt [ns]/280). These parameters are a little different from those used in subsection 3.1 according to the following considerations. The relatively large radius (4 mm) of foam converter can help to avoid the cylindrical shock directly impact onto the capsule. The length of load is reduced to save the simulation time, while it is still long enough to make the radiation loss at the two ends do not lower the radiation temperature on pellet poles significantly. The relatively low foam density (5 mg/cm^3), the same as that used in Sandia's dynamic hohlraum driven capsule implosions [31], is chosen to make the thermal wave propagate much faster than the shock, so that the testing pellet has more chances to be imploded spherically by the radiation before it is compressed by the cylindrical shock.

Different grids are used for different objects. The pellet is divided into quadrangular cells organized in spherical form to avoid numerical asymmetry. The tungsten plasma is divided into regular rectangles which fit the cylinder geometry best. The mesh for plastic foam is composed of irregular triangles, providing smooth transition between the spherical pellet and cylindrical array plasma.

The radiation temperature distributions at different time are presented in Fig. 5. The shock front is identified through the accumulation of grid. It is shown that the tungsten plasma has already collided with the foam at 155 ns. The shock positions in the foam (shock S1) and thermal wave are 2.12 mm and 0.50 mm, respectively. It is found that the pellet is first ablated on the equator since the cylindrical thermal wave travels inward. At the time of 158 ns, thermal wave has already reached the axis, and the pellet is ablated by an almost uniform radiation field, with a radiation temperature about 90 eV. This temperature is a little lower than that without a pellet inside due to that the pellet absorbs some radiation energy in the hohlraum. The radiation temperature will increase to 100 eV if we decrease pellet density to 5 mg/cm^3, the same density without the pellet. The cylindrical shock (S1) in the foam is just about to arrive at the cylinder axis at 162.6 ns, the radiation temperature around the pellet rises to 150 eV at this time due to the shock heating and compression work (pdV). One

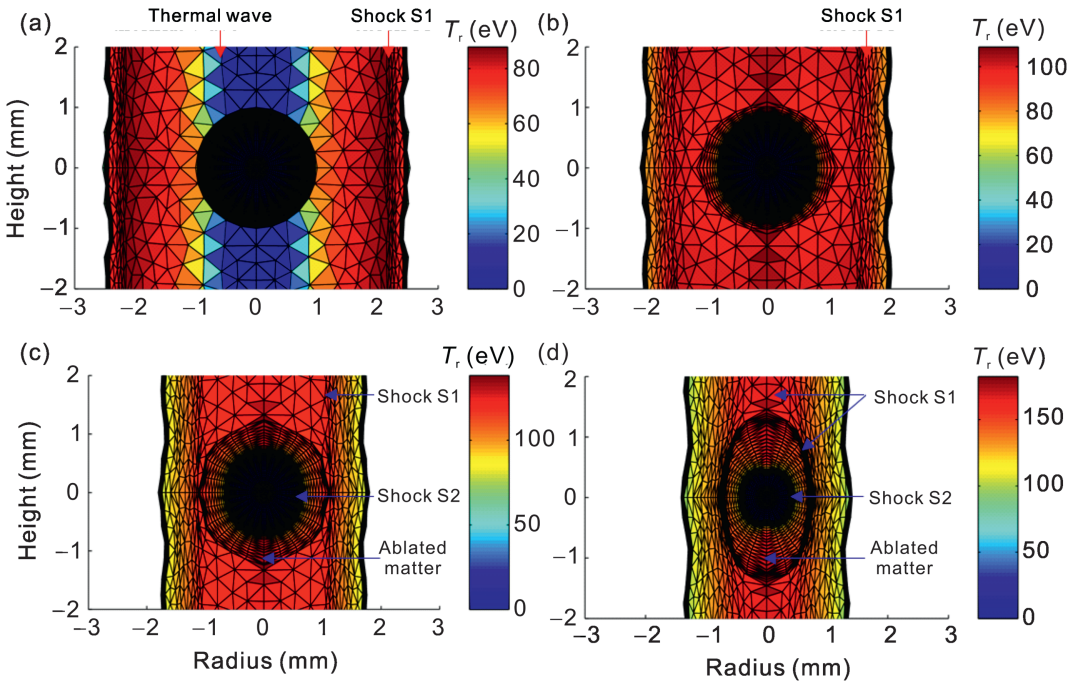

Fig. 5. Radiation temperature distribution at different times. (a) 155 ns, (b) 158 ns, (c) 160 ns, (d) 162.6 ns.

can also notice that the front of shock S1 in the foam turns into a bow shape due to the interaction with the ablated matter.

The density distributions corresponding to the time in Fig. 5 are presented in Fig. 6. It is shown that the spherical pellet becomes an ellipsoid due to that the integrated radiation flux is larger on equator than that on poles before 157.4 ns. The ratio of pellet radii on equator and poles ($R_{\text{equator}}/R_{\text{pole}}$) at 162.6 ns is 0.44/0.49 = 0.90, when the shock S1 in the foam is about to reach the hohlraum center. When the shock S1 collapses to the cylinder axis, regions of high matter pressure (>5 Mbar) and high radiation temperature (>200 eV) will be generated, resulting in severe compression of the pellet in axial direction on the poles. From Fig. 6, one can infer that the shock S1 in the foam slows down from 24.7 cm/μs to 18.8 cm/μs,

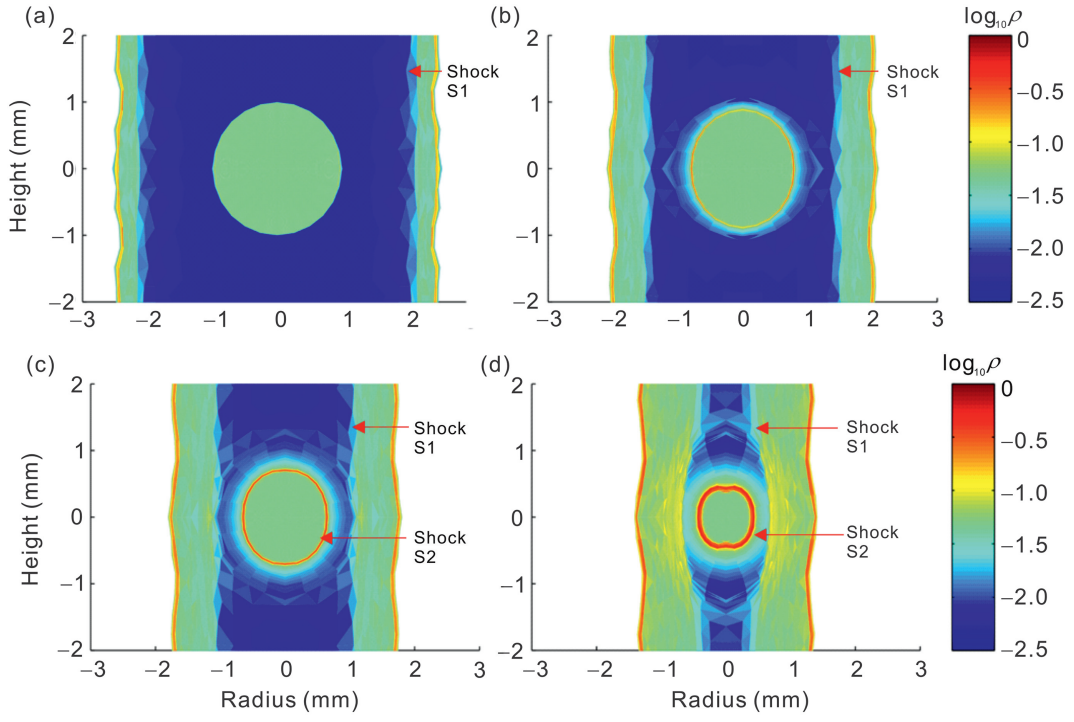

Fig. 6. Density distribution at different times (the same scale, in mg/cc). (a) 155 ns, (b) 158 ns, (c) 160 ns, (d) 162.6 ns.

indicating that the ablative standoff effect [19,32] produced by the interaction between the outward ablated matter and the incoming shock S1 is already obvious for Julong-I facility.

The above calculation results show that pellet implosion with good spherical symmetry cannot be achieved when the load parameters are not optimized. There are at least two key points to obtain spherical implosion for Z-pinch dynamic hohlraum driven fusion. First, the radiation temperature around the pellet should be uniform both before and after the thermal wave reaches the cylinder axis, so that the integrated radiation flux on the pellet surface has a good spherical symmetry. Second, the pellet implosion should be isolated from the incoming cylindrical shock before ignition happens. If sufficient large drive current (e.g. 60 MA) is available, these two conditions may be satisfied due to accessible higher radiation temperature (~300 eV) [33]. Higher radiation temperature is helpful to shorten the time for the thermal wave traveling from the pellet equator to the pellet poles and isolate the cylindrical shock in the foam with ablative standoff effect. For Julong-I facility with a peak drive current of 8 MA, we will show that the radiation uniformity can also be improved by using the concept of quasi-spherical implosion in the next subsection.

3.3. Improving hohlraum radiation uniformity with quasi-spherical implosion

The initial configuration is illustrated in Fig. 7. The tungsten wire array plasma is shaped to get the required quasi-spherically implosion, which can be realized by charging the array electrostatically and adjusting the electrode gap in experiments, as shown by Chu and Zhang et al. [23,24]. The radial coordinate of the tungsten wire array plasma is modulated as $r = r_0\,[1 + 0.008\cos(\pi z\ [\mathrm{mm}]/5)]$, the radial coordinate of plastic foam is modulated as $r = r_0\,[1 + 0.07\cos(\pi z\ [\mathrm{mm}]/5)]$, where r is the radius of each node, r_0 is the original radius of each node, z is the axial coordinate. It should be noted that the amplitude of wire-array position modulation is not only limited to 0.008, both the plastic foam and the electrodes can be shaped if larger modulation is required. However, due to the inherent defect of current Lagrangian code MULTI-2D, the grid will be too distorted or even overlapped when the modulation is very large, so we do not attempt to give configurations that can be used in experiment directly herein. Simulations including shaped array, foam and electrodes will be performed in the future, when new version of code MULTI-2D with a second order Arbitrary Lagrangian Eulerian (ALE) scheme is available.

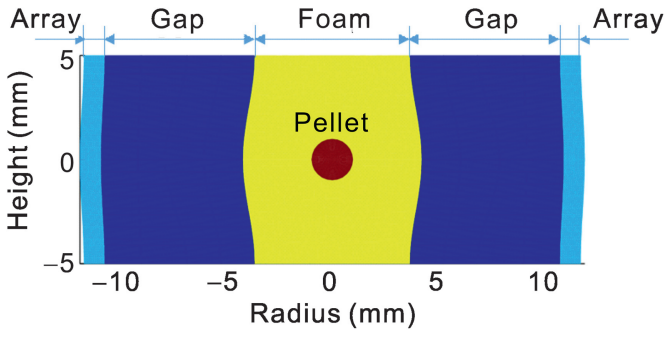

Fig. 7. Schematic of quasi-spherical hohlraum driven pellet implosion.

The density distributions at different time are displayed in Fig. 8. It is shown that the tungsten plasma has already impacted onto the plastic foam at 154 ns. Because the magnetic field depends inversely on the radius ($B = \mu_0 I/2\pi r$), the driving forces, mainly the magnetic pressures ($p = B^2/2\mu_0$), on the two ends are larger than that on the equator. Thus, compared with the cylindrical implosion, the tungsten plasmas on the two ends move faster while the plasma on the equator moves slower, making the shape of tungsten plasma turn into quasi-spherical rather than cylindrical. A quasi-spherical shock wave (S1) launched by the collision of tungsten plasma and plastic foam can be observed at this time as well. The tungsten plasma starts to collide with the low density plastic foam near the initial foam radius at 146 ns. However, because the tungsten plasma still has high imploding velocity after the collision (~1.70×10^7 cm/s at 154 ns), the quasi-spherical shock S1 does not significantly separate from the imploding tungsten plasma until the time of 158 ns. At 158 ns, the radiating shock wave (S1) is still far away from the pellet but the thermal wave has already arrived at the pellet surface as shown in Fig. 9. At 160 ns, significant pellet ablation and a spherical converging shock (S2) driven by the radiation

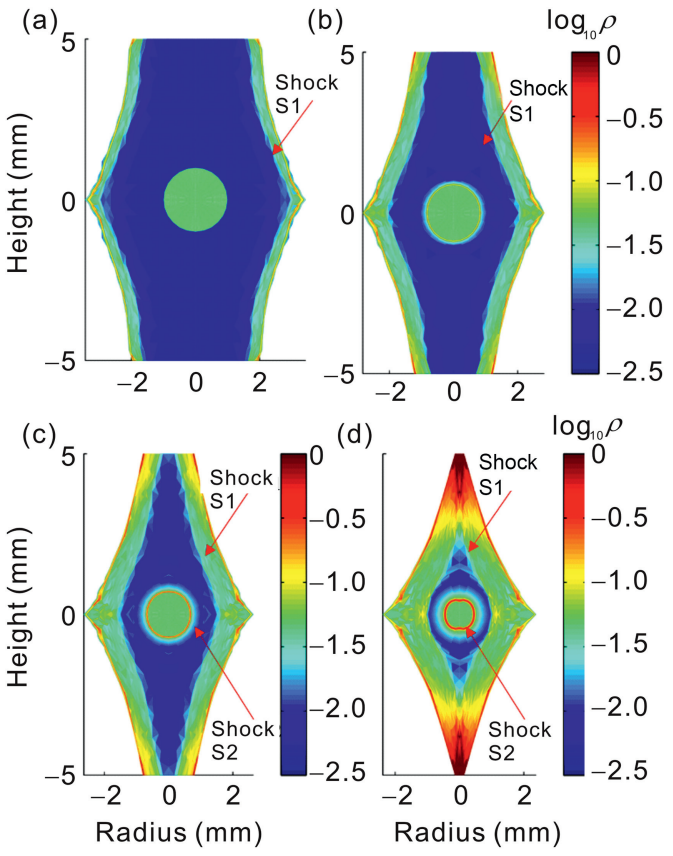

Fig. 8. Density distribution at different time (in mg/cm^3). (a) 154 ns, (b) 158 ns, (c) 160 ns, (d) 162.6 ns.

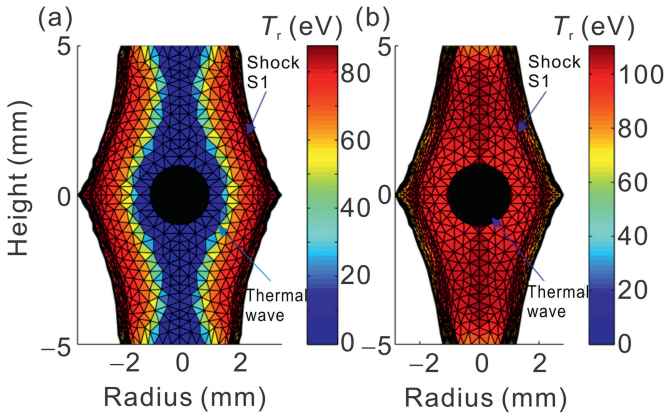

Fig. 9. Radiation temperature distribution at (a) 154 ns and (b) 158 ns.

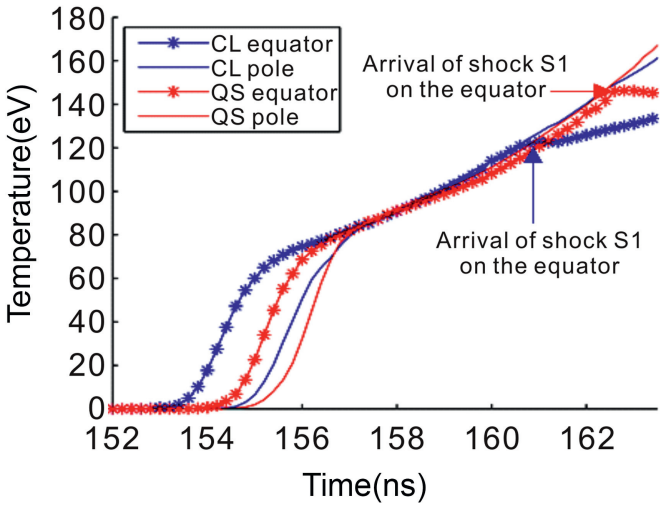

Fig. 10. Evolution of radiation temperature for cylindrical hohlraum (CL) and quasi-spherical hohlraum (QS).

ablation can be observed. At 162.6 ns, the ablated matter of pellet has collided with the shock (S1) on equator, but the spherical shock S2 in the pellet still preserves good symmetry. As a comparison, the ratios of pellet radii on equator and poles ($R_{equator}/R_{pole}$) at 162.6 ns are 0.48/0.49 = 0.98 and 0.44/0.49 = 0.90 for quasi-spherical and cylindrical implosions respectively, indicating clear advantage of quasi-spherical hohlraum on the improvement of radiation uniformity.

To analyze why a better radiation uniformity is achieved in the quasi-spherical hohlraum, we plot the radiation field distributions at different time in Fig. 9. It is shown that a shock wave and a thermal wave have been launched at 154 ns, and both of them are quasi-spherical, because the Z-pinch plasma is quasi-spherical when it collides with the plastic foam. This quasi-spherical shape is beneficial for spherical pellet implosion. First, the thermal wave is easier to arrive at the pellet surface simultaneously, so that the integrated radiation flux is more uniform before the thermal wave reaches the axis. As can be seen at 158 ns, the pellet remains spherical, in contrast that significant implosion asymmetry can be observed in the cylindrical hohlraum (Fig. 5(b)). Second, the shock in the foam is farther away from the pellet on the equator, so that there is more time for the pellet to be ablated by the radiation field before compressed hydro-dynamically by the cylindrical shock in the foam. Besides, since the hohlraum heat source locates at the region between shock front and array plasma, the radiation incident on the pellet is more uniform in the stand point of the view factor model [2]. The view factor of each point on the pellet is a solid angle weighted integral over visible heat source.

Evolutions of radiation temperature on the original position of pellet equator (r = 1 mm, z = 0 mm) and pellet pole (r = 0 mm, z = 1 mm) for cylindrical hohlraum (CL) and quasi-spherical hohlraum (QS) are plotted in Fig. 10. It is shown that the radiation temperature on pellet surface differs little for these two cases during 157.2 ns–160.6 ns, due to array plasma on equator of QS hohlraum implodes slower than that of cylindrical hohlraum (e.g. at 160 ns). However, two obvious advantages can be observed thanks to the use of quasi-spherical implosion. First, the time interval between the thermal waves reaching the equator and pole decreases from 1.4 ns to 0.8 ns. Second, the time of cylindrical shock (shock S1) in the foam arrives at the equator increases from 160.6 ns to 162.6 ns, delaying the pellet to be compressed by the cylindrical shock directly.

4. Conclusions

The radiation uniformity of Z-pinch dynamic hohlraum on Julong-I facility (7–8 MA) is numerically investigated by the code MULTI-2D with a new developed magnetic field package. It is found that radiation field in the hohlraum center without a pellet inside will become uniform after a transition of ~2.0 ns, and the radiation temperature can achieve over 100 eV before the shock arrives at the axis. The implosion of a testing pellet made of CH foam indicates that the spherical symmetry of pellet may be destroyed by the transition phase of radiation field and the incoming of cylindrical shock in the foam. The radiation uniformity could be improved by replacing the cylindrical hohlraum with a quasi-spherical hohlraum, where the thermal wave is easier to reach the pellet surface at the same time, and the mechanically compression by the cylindrical shock in the foam can be delayed. For the load parameters used in this paper, the ratio of pellet radii on the equator and poles ($R_{equator}/R_{pole}$) could be increased from 0.90 to 0.98 with the help of quasi-spherical hohlraum. In the future, we will develop a 2D hydrodynamic code with a second order ALE scheme to study the radiation uniformity of Z-pinch dynamic hohlraum with present of a real fusion capsule and shaped metal electrodes.

Conflict of interest

All authors declare no conflicts of interest.

Acknowledgments

The authors wish to thank Professor Ning Ding, Cheng Ning, and Delong Xiao for lots of useful discussions during

this work. This work was supported by the National Natural Science Foundation of China (Nos. 11374357, 11475153, 11705282, and 11475260), Science Challenge Project (No. TZ2018001), Research Project of NUDT (Grant No. ZK16-03-29), the Spanish Ministerio de Economia y Competivida project (No. ENE2014-54960-R), and the EUROfusion Consortium project AWP15-ENR-01/CEA-02.

References

[1] J.D. Lindl, P. Amendt, R.L. Berger, S.G. Glendinning, S.H. Glenzer, et al., The physics basis for ignition using indirect-drive targets on the National Ignition Facility, Phys. Plasmas 11 (2004) 339−491.

[2] Ke Lan, Jiu Liu, Zhichao Li, Xufei Xie, Wenyi Huo, et al., Progress in octahedral spherical hohlraum study, Matter. Radiat. Extrem. 1 (2016) 8−27.

[3] S. Kawata, T. Karino, A.I. Ogoyski, Review of heavy-ion inertial fusion physics, Matter. Radiat. Extrem. 1 (2016) 89−113.

[4] C. Olson, G. Rochau, S. Slutz, C. Morrow, R. Olson, et al., Development path for Z-pinch IFE, Fusion Sci. Technol. 47 (2005) 633−640.

[5] R.B. Spielman, C. Deeney, G.A. Chandler, M.R. Douglas, D.L. Fehl, et al., Tungsten wire-array Z-pinch experiments at 200 TW and 2 MJ, Phys. Plasmas 5 (1998) 2105−2111.

[6] C.L. Ruiz, G.W. Cooper, S.A. Slutz, J.E. Bailey, G.A. Chandler, et al., Production of thermonuclear neutrons from deuterium-filled capsule implosions driven by Z-pinch dynamic hohlraums, Phys. Rev. Lett. 93 (2004) 015001.

[7] G.A. Rochau, J.E. Bailey, G.A. Chandler, G. Cooper, G.S. Dunham, et al., High performance capsule implosions driven by the Z-pinch dynamic hohlraum, Plasma Phys. Contr. Fusion 49 (2007) B591.

[8] W.A. Stygar, T.J. Awe, J.E. Bailey, N.L. Bennett, E.W. Breden, et al., Conceptual designs of two petawatt-class pulsed-power accelerators for high-energy-density-physics experiments, Phys. Rev. ST Accel. Beams 18 (2015) 110401.

[9] R.W. Lemke, J.E. Bailey, G.A. Chandler, T.J. Nash, S.A. Slutz, et al., Amplitude reduction of nonuniformities induced by magnetic Rayleigh−Taylor instabilities in Z-pinch dynamic hohlraums, Phys. Plasmas 12 (2005) 012703.

[10] S.A. Slutz, K.J. Peterson, R.A. Vesey, R.W. Lemke, J.E. Bailey, et al., Integrated two-dimensional simulations of dynamic hohlraum driven inertial fusion capsule implosions, Phys. Plasmas 13 (2006) 102701.

[11] Jianjun Deng, Weiping Xie, Shuping Feng, Meng Wang, Hongtao Li, et al., From concept to reality—A review to the primary test stand and its preliminary application in high energy density physics, Matter. Radiat. Extrem. 1 (2016) 48−58.

[12] Delong Xiao, Shunkai Sun, Chuang Xue, Yang Zhang, Ning Ding, Numerical studies on the formation process of Z-pinch dynamic hohlruams and key issues of optimizing dynamic hohlraum radiation, Acta Phys. Sin. 64 (2015) 235203.

[13] Ning Ding, Yang Zhang, Delong Xiao, Jiming Wu, Zihuan Dai, et al., Theoretical and numerical research of wire array Z-pinch and dynamic hohlraum at IAPCM, Matter. Radiat. Extrem. 1 (2016) 135−152.

[14] Xianbin Huang, Xiaodong Ren, Jiakun Dan, Kunlun Wang, Qiang Xu, et al., Radiation characteristics and implosion dynamics of Z-pinch dynamic hohlraums performed on PTS facility, Phys. Plasmas 24 (2017) 092704.

[15] Shijian Meng, Qingyuan Hu, Jiaming Ning, Fan Ye, Zhanchang Huang, et al., Measurement of axial radiation properties in Z-pinch dynamic hohlraum at Julong-1, Phys. Plasmas 24 (2017) 014505.

[16] Fuyuan Wu, Rafael Ramis, Zhenghong Li, Yanyun Chu, Jianlun Yang, Numerical simulation of the interaction between Z-pinch plasma and foam converter using code MULTI, Fusion Sci. Technol. (2017), https://doi.org/10.1080/15361055.2017.1347458.

[17] R. Ramis, J. Meyer-ter-Vehn, J. Ramírez, MULTI2D—a computer code for two-dimensional radiation hydrodynamics, Comput. Phys. Commun. 180 (2009) 977−994.

[18] Fuyuan Wu, Rafael Ramis, Zhenghong Li, A conservative MHD scheme on unstructured Lagrangian grids for Z-pinch hydrodynamic simulations, J. Comput. Phys. (2017), https://doi.org/10.1016/j.jcp.2017.12.014.

[19] S.A. Slutz, M.R. Douglas, J.S. Lash, R.A. Vesey, G.A. Chandler, et al., Scaling and optimization of the radiation temperature in dynamic hohlraums, Phys. Plasmas 8 (2001) 1673−1691.

[20] T.J. Nash, D.H. McDaniel, R.J. Leeper, C.D. Deeney, T.W.L. Sanford, Design, simulation, and application of quasi-spherical 100 ns Z-pinch implosions driven by tens of mega-amperes, Phys. Plasmas 12 (2005) 052705.

[21] V.P. Smirnov, S.V. Zakharov, E.V. Grabovski, Increase in radiation intensity in a quasi-spherical double liner/dynamic hohlraum system, JETP Lett. 81 (2005) 442−447.

[22] E.V. Grabovskii, A.N. Gritsuk, V.P. Smirnov, V.V. Aleksandrov, G.M. Oleinik, et al., Current implosion of quasi-spherical wire arrays, JETP Lett. 89 (2009) 315−318.

[23] Yanyun Chu, Zhenghong Li, Jianlun Yang, Ning Ding, Rongkun Xu, et al., Simulation of the quasi-spherical wire-array implosion dynamics based on a multi-element model, Plasma Phys. Contr. Fusion 54 (2012) 105020.

[24] Yang Zhang, Ning Ding, Zhenghong Li, Rongkun Xu, Dingyang Chen, et al., Realization of quasi-spherical implosion using pre-shaped prolate wire arrays with a compression foam target inside, Phys. Plasmas 22 (2015) 020703.

[25] R. Ramis, J. Meyer-ter-Vehn, MULTI-IFE—A one-dimensional computer code for Inertial Fusion Energy (IFE) target simulations, Comput. Phys. Commun. 203 (2016) 226−237.

[26] Fuyuan Wu, Yanyun Chu, Fan Ye, Zhenghong Li, Jianlun Yang, One-dimensional numerical investigation on the formation of Z-pinch dynamic hohlraum using the code MULTI, Acta Phys. Sin. 66 (2017) 215201.

[27] T.W.L. Sanford, G.O. Allshouse, B.M. Marder, T.J. Nash, R.C. Mock, et al., Improved symmetry greatly increases X-ray power from wire-array Z-pinches, Phys. Rev. Lett. 77 (1996) 5063.

[28] S.V. Lebedev, F.N. Beg, S.N. Bland, J.P. Chittenden, A.E. Dangor, et al., Snowplow-like behavior in the implosion phase of wire array Z pinches, Phys. Plasmas 9 (2002) 2293.

[29] A.A. Esaulov, V.L. Kantsyrev, A.S. Safronova, A.L. Velikovich, I.K. Shrestha, et al., Wire ablation dynamics model and its application to imploding wire arrays of different geometries, Phys. Rev. E 86 (2012) 046404.

[30] K. Lan, Y. Zhang, Theoretical studies of aluminum wire array Z-pinch implosions with varying masses and radii, Eur. Phys. J. Appl. Phys. 19 (2002) 103.

[31] J.E. Bailey, G.A. Chandler, S.A. Slutz, G.R. Bennett, G. Cooper, et al., X-ray imaging measurements of capsule implosions driven by a Z-pinch dynamic hohlraum, Phys. Rev. Lett. 89 (2002) 095004.

[32] Delong Xiao, Shunkai Sun, Yingkui Zhao, Ning Ding, Jiming Wu, et al., Numerical investigation on target implosions driven by radiation ablation and shock compression in dynamic hohlraums, Phys. Plasmas 22 (2015) 052709.

[33] T.J. Nash, M.S. Derzon, G.A. Chandler, R. Leeper, D. Fehl, et al., High-temperature dynamic hohlraums on the pulsed power driver Z, Phys. Plasmas 6 (1999) 2023−2029.